Metasurface Antennas: Efficiency versus Bandwidth

Modeste Bodehou, Marco Faenzi, David Gonzalez-Ovejero, Stefano Maci, Christophe Craeye, Enrica Martini

Metasurface Antennas: Efficiency versus Bandwidth

Modeste Bodehou*, Marco Faenzi†, David González-Ovejero‡, Stefano Maci†, Christophe Craeye*, Enrica Martini†
*Université catholique de Louvain: ICTEAM Institute, Place du Levant, 3, 1348, Louvain-la-Neuve, Belgium
†Department of Information Engineering and Mathematics, University of Siena, 53100 Siena, Italy
‡Univ Rennes, CNRS, IETR (Institut d'Électronique et de Télécommunications de Rennes), UMR 6164, 35000 Rennes, France.
modeste.bodehou @uclouvain.be

***Abstract*—Two methods are proposed for the accurate and fast analysis of the efficiency of arbitrarily modulated metasurface (MTS) antennas. The surface current on the MTS is expanded into entire-domain basis functions. The first method uses a Fourier-Bessel basis and relies on the Poynting theorem, while the second approach is based on the calculation of the surface-wave residue with a Gaussian-Ring expansion for the current. Both methods allow one to compute the efficiency of MTS antennas in a few minutes, which represents a drastic reduction of the computation time in comparison with any commercial software. The algorithms are then used to analyze the frequency dependence of the efficiency of MTS antennas in two different cases: 1) anisotropic MTS with uniform periodicity, 2) anisotropic MTS with non-uniform periodicity. The latter case corresponds to an active region MTS and provides a larger bandwidth. Validation with commercial software and measurements data is provided.**

***Index Terms*—metasurface, efficiency, bandwidth.**

I. Introduction

It is well known that metamaterials (MTMs) and metasurfaces (MTSs) generally suffer from bandwidth limitations due to the frequency dispersion of the propagating waves [1]. In many communication and radar systems, a minimum bandwidth is required to satisfy the desired data rate or to provide a sufficient resolution. Despite several advantages provided by MTS antennas (low profile, low cost, low losses), their bandwidth may be limited, mainly due to a mismatch between the wavelength of the supported surface-wave (SW) and the period of the modulation. Indeed, those antennas are designed to mimic a modulated surface impedance at a given frequency [2]-[8]. The role of the feed consists of exciting a SW in the slab, which progressively looses its energy as a leaky-wave (LW). The LW radiation results from the interaction between the SW and the impressed impedance profile. When the frequency of operation is changed, the periodicity of the modulation rapidly becomes inconsistent with the supported SW mode, thereby limiting the bandwidth. This issue has been recently addressed in [9] by an active region radiation concept. The idea is to impose a variation of the modulation period in the radial direction such that, at a given frequency, a given annular region of the antenna radiates. This allows one to enlarge the antenna bandwidth, at the expense of a lower aperture efficiency. However, since those structures are LW antennas, one should ensure that the power carried by the SW is radiated before reaching the periphery of the antenna. Otherwise, significant diffraction/reflection effects can occur at the antenna rim, which can strongly impact the antenna performance. This calls for the definition of a conversion efficiency, which represents the ratio between the radiated power, assuming an infinite slab, and the power provided by the feed. When analyzing those antennas printed on an infinite slab as commonly done in Method of Moments (MoM) approaches [10]-[12], scattering at the rim is not taken directly into account and a non-negligible SW power may be carried away by the infinite slab. Therefore, it is important for the antenna designer to have a rapid evaluation of the conversion efficiency, namely the ratio between the radiated power and the total power delivered by the feed, and the aperture efficiency, so as to optimize the global efficiency of the antenna before proceeding to realization. This paper provides two effective (fast and accurate) methods for the computation of the efficiency of MTS antennas. With those methods, we analyze the frequency variation of the efficiency when the bandwidth of the antenna is getting larger. The paper is structured as follows. Section II is devoted to the MTS modeling, Sections III and IV discuss the computation of the powers required for the derivation of the efficiency. Section V analyzes the efficiency versus frequency response of MTS antennas and Section VI concludes the paper.

II. MTS Modeling and Power Balance

Let us consider a circular domain MTS antenna of radius a, whose cut is represent in Fig. 1. The antenna is fed at the center with a source point. The MTS layer is modeled as a sheet impedance distribution and lays on an infinitely extended

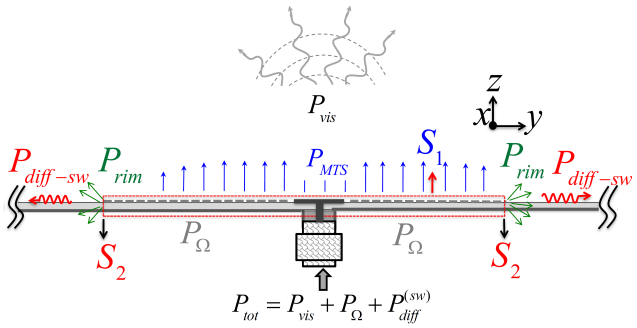

Fig. 1. Power contributions for a finite MTS over an infinite grounded substrate.

substrate. Assuming a perfect matching of the feed, the power delivered to the antenna (P_{tot}) is partially radiated (P_{vis}), partially lost in the substrate (ohmic power losses (P_Ω)) and partially reflected/diffracted at the substrate rim (P_{diff}). Since the losses in MTS antennas are negligible at low frequency (< 30 GHz) [4], one can simply write the power balance as

$$P_{tot} = P_{vis} + P_{diff}^{sw} \ . \tag{1}$$

This paper aims at accurately and rapidly estimating the power contributions P_{tot}, P_{vis} and P_{diff}, as well as the aperture efficiency of the antenna. First, the equivalent surface current distribution on the MTS is computed with Fourier-Bessel basis functions (FBBF) [10] or Gaussian-Ring basis functions (GRBFs) [11] using the MoM. The first method (based on the Poynting theorem) enables the computation of P_{vis}, P_{tot} and then derives P_{diff} from equation (1). The second method, based on the residue theorem, computes P_{vis}, P_{diff}, and then deduces P_{tot} from (1). In both methods, P_{vis} is computed directly in spectral domain using the close form spectrum of the FBBFs or GRBFs [13]. In the following, the computation of P_{tot} and P_{diff} are detailed.

III. Total power calculation based of the Poynting theorem

From the Poynting theorem and in absence of losses, the power delivered by the feed can be calculated after integrating the flux of the Poynting vector along any closed surface including the feed. We suggest the surface represented in red line in Fig. 1. This surface comprises the MTS layer, the rim as well as the ground plane. The total power delivered by the feed can then be written as:

$$\begin{aligned} P_{tot} &= \frac{1}{2} Re \left\{ \iint_{S_1} \mathbf{E}_t \times \mathbf{H}_t^* \ . \ \hat{\mathbf{z}} \ dS + \iint_{S_2} \mathbf{E} \times \mathbf{H}^* \ . \ \hat{\boldsymbol{\rho}} \ dS \right. \\ &= P_{MTS} + P_{rim}, \end{aligned} \tag{2}$$

where P_{MTS} and P_{rim} are illustrated in Fig. 1. t means the tangential part. $\mathbf{E}$ and $\mathbf{H}$ are the electric field and the magnetic field respectively. $\hat{\boldsymbol{\rho}}$ is the radial unit vector and Re is the real part operator.

A. MTS contribution

The MTS contribution is written as:

$$P_{MTS} = \frac{1}{2} Re \left\{ \iint_{S_1} E_x \ . \ H_y^* - E_y \ . \ H_x^* \ dS \right\}, \tag{3}$$

To compute the electric field, we calculate the tested electric field on the surface from the MoM matrix $[\mathbf{Z}_G^E]$ and the MoM excitation vector $[\mathbf{V}^E]$ as:

$$[\mathbf{E}_t] = [\mathbf{Z}_G^E] \ [\mathbf{I}] - [\mathbf{V}^E], \tag{4}$$

Since the FBBFs are orthogonal on the MTS aperture (see orthogonality relation in [10]), the electric field in the Fourier-Bessel basis is derived from the tested field by simple renormalization. A similar procedure is used for the computation of the magnetic field. This allows one to express integral (3) as a double summation over all the basis functions:

$$P_{MTS} = \frac{1}{2} \sum_{n=-N}^{N} \sum_{m=1}^{M} K(m,n) Re \left\{ e_{mn}^x h_{mn}^{y*} - e_{mn}^y h_{mn}^{x*} \right\}. \tag{5}$$

where index mn identifies each basis function, e_{mn} and h_{mn} correspond to the electric field and the magnetic field coefficients respectively and $K(m,n)$ is the normalization factor.

B. Rim contribution

For a quasi-TM mode, the rim contribution can be developed as

$$P_{rim} \approx -\frac{1}{2} Re \left\{ \iint E_z(\rho = a) \ H_\phi^*(\rho = a) \ d\phi \ dz \right\} \tag{6}$$

where ρ and ϕ are the classical cylindrical coordinates. The z component of the electric field is split into three contributions corresponding to each Cartesian direction of the current (E_{zx}, E_{zy}, and E_{zz}). In the same way, we defined H_{xx}, H_{xy}, H_{xz}, H_{yx}, H_{yy}, and H_{yz}.

1) Evaluation of E_{zx}: The z component of the electric field due to the x-directed current (known in the FBBF basis) is computed spectrally with the pertaining spectral Green's function $\widetilde{G}_{zx}^{EJ}$ through inverse Fourier transform.

$$E_{zx} = \frac{1}{4\pi^2} \sum_{m,n} i_{mn}^x \iint \widetilde{G}_{zx}^{EJ} \widetilde{R}_{mn} e^{-j(k_x x + k_y y)} dk_x dk_y \tag{7}$$

The spectral Green's function $\widetilde{G}_{zx}^{EJ}$ and the FBBF Fourier transform $\widetilde{R}_{mn}$ can be structurally written as $\widetilde{g}_{zx}^E(k_\rho) \cos\alpha$, and $\widetilde{F}_{mn}(k_\rho) e^{-jn\alpha}$ respectively. Inserting the latter expressions in (7), and using a cylindrical spectral coordinates (k_ρ, α), expression (7) can be rewritten as

$$\begin{aligned} E_{zx} = \frac{1}{4\pi^2} \sum_{m,n} i_{mn}^x \int_0^\infty \widetilde{g}_{zx}^E \ \widetilde{F}_{mn} \int_0^{2\pi} \cos\alpha \ e^{-jn\alpha} \\ e^{-jk_\rho \rho \cos(\phi - \alpha)} \ d\alpha \ k_\rho \ dk_\rho \end{aligned} \tag{8}$$

Then, one can integrate in closed form along α:

$$\begin{aligned} E_{zx} = \frac{1}{4\pi^2} \sum_{m,n} i_{mn}^x \int_0^\infty \widetilde{g}_{zx}^E \ \widetilde{F}_{mn} \ j \left[f_n^0(k_\rho \rho, \phi, 1) - \right. \\ \left. f_n^0(k_\rho \rho, \phi, -1) \right] k_\rho \ dk_\rho \end{aligned} \tag{9}$$

where we defined the function f_n^0 as

$$f_n^0(k_\rho \rho, \phi, i) = \pi j^n e^{-j(n+i)\phi} J_{n+i}(-k_\rho \rho) \tag{10}$$

and $J_n(x)$ represents the first kind Bessel function of order n. We simplify the notations by defining the following functions:

$$f_{mn}^a(k_\rho \rho, \phi, -1) = -j \ f_n^0(k_\rho \rho, \phi, -1) \ \widetilde{g}_{zx}^E \ \widetilde{F}_{mn} \tag{11}$$

$$f_{mn}^b(k_\rho \rho, \phi, 1) = j \ f_n^0(k_\rho \rho, \phi, 1) \ \widetilde{g}_{zx}^E \ \widetilde{F}_{mn} \tag{12}$$

Then, according to (11), and (12), E_{zx} can be structurally written as

$$E_{zx} = \frac{1}{4\pi^2}\sum_{m,n} i^x_{mn}\int_0^\infty \left[f^a_{mn}(k_\rho\rho,\phi,-1)+ f^b_{mn}(k_\rho\rho,\phi,1)\right] k_\rho\, dk_\rho \tag{13}$$

Expression (13) is a harmonic representation of the fields in the the azimuthal direction. The same thing is done for all the other components of the electric and magnetic fields. This enables a harmonic azimuthal representation of each component of the total electric field, and hence an analytical integration along the azimuthal direction. Moreover, integrals along k_ρ are separable and can be pre-computed, which significantly accelerates the computation. Integration along z is carried out with very few sampling points (about 4) since the integrand along z is relatively smooth. Details regarding the formulation can be found in [13], [14].

IV. SW Power Computation Based on the Calculation of the SW Residue

This approach is based on the evaluation of the residual (i.e. not radiated) SW power through the calculation of the residue of the current at the SW pole of the bare grounded slab. This calculation is performed in an extremely efficient way through a closed-form expression involving the spectrum of the current. The derivation starts from the following expression for the z-component of the spectrum of the aperture electric field:

$$\widetilde{E}_z(k_\rho,\alpha) = \sum_n \widetilde{E}_{zn}(k_\rho)e^{-jn\alpha} \tag{14}$$

which contains both the contribution of the currents in the MTS and the direct contribution of the feed, which only contributes to the 0-indexed term, due to its axial symmetry. It is noted that this form is automatically available if GRBFs or FBBFs are used for MTS current representation. The spatial field is obtained by taking the inverse Fourier transform of the expression in (14). For $\rho > a$, where a is the radius of the MTS, this can be divided into two contributions: the radiated field and the SW field. This latter is given by the contribution of the residue at the SW pole of the bare grounded slab, β_0^{sw}, and reads

$$E_z^{SW} = -\frac{j}{2}e^{-j\frac{\pi}{4}}\sqrt{\frac{2\beta_0^{sw}}{\pi\rho}}e^{-j\beta_0^{TM}\rho}\sum_n R_n e^{-jn\phi} \tag{15}$$

where we have assumed $\beta_0^{sw}\rho \gg 1$ and

$$R_n = \lim_{k_\rho\to\beta_0^{sw}}(k_\rho-\beta_0^{sw})\,\widetilde{E}_{zn} = \widetilde{J}_n^{TM}(\beta_0^{sw})\,R_{GF} + \delta_{n,0}R_{feed} \tag{16}$$

In (16), $\widetilde{J}_n^{TM}(\beta_0^{sw}) = \int_0^{2\pi}\widetilde{J}^{TM}(\beta_0^{sw},\alpha)\,e^{jn\alpha}d\alpha$, R_{GF} is the residue of the Green's function relating the TM currents on the MTS to the vertical electric field on top of the slab and R_{feed} is the residue of the field radiated by the feed on the bare slab. From (15), taking into account the local structure of the SW electromagnetic field, the real part of the relevant Poynting vector is derived, and integrated over a cylindrical surface surrounding the radiating aperture and extending from the ground plane to infinity, to obtain the following expression for the residual SW power

$$P^{sw}_{diff} = \frac{\omega\epsilon_0}{4\epsilon_r}\left[\frac{\tan(k_{zd}h)}{k_{zd}} + \frac{h}{\cos^2(k_{zd}h)} + \frac{\epsilon_r}{\alpha_{za}}\right]\sum_n |R_n|^2 \tag{17}$$

where ϵ_0 is the free-space permittivity, ϵ_r is the relative permittivity of the substrate, $\omega = 2\pi f$ is the angular frequency, h is the slab thickness, $k_{zd} = \sqrt{k_0^2\epsilon_r - (\beta_0^{sw})^2}$ and $\alpha_{za} = \sqrt{(\beta_0^{sw})^2 - k_0^2}$. Notice that the evaluation of (17) only requires the knowledge of the residues in (16), which can be calculated for any given current spectrum. However, the general expression can be also specialized to the particular case of a given current representation. For instance, if GRBFs are used to represent MTS currents, it results

$$\widetilde{J}_n^{TM}(\beta_0^{sw}) = \pi j^n\sum_{m=1}^{M}\left\{\left[ji^x_{m,n+1}+i^y_{m,n+1}\right]\Phi_{m,n+1}(\beta_0^{sw}) + \left[i^y_{m,n-1}-i^x_{m,n-1}\right]\Phi_{m,n-1}(\beta_0^{sw})\right\} \tag{18}$$

where the Φ functions are reported in [11].

V. Results

A. Validation of the two methods

This section provides a numerical validation (with the commercial software FEKO [15]) of the two methods detailed in Section III and Section IV. We consider a MTS antenna radiating a broadside pencil beam, which parameters are described in Section V.A of [11]. Fig. 2 shows the efficiency results for various modulation indices. One can see that,

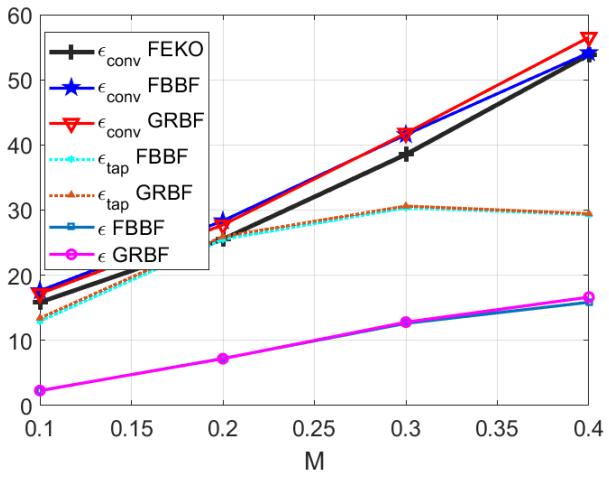

Fig. 2. Validation of the efficiency results for different modulation indices. The global efficiency ϵ is the product between the aperture (tapering) efficiency ϵ_{tap} and the conversion efficiency ϵ_{conv}.

although those two methods are based on quite different formalisms and that they have been demonstrated here with two different sets of basis functions, the efficiency results are very similar and follow well the FEKO solution. The slight

difference with respect to FEKO may be explained by the feeder modeling. In terms of computation time, the Poynting theorem based method and the residue based method take respectively 2.5 min and 1.1 min on a conventional computer, while FEKO simulations require 2.4 hours. This represents a drastic reduction of the computation time.

B. Efficiency versus frequency analysis

A MTS antenna with uniform periodicity and designed to generate a broadside beam at 29.75 GHz is now considered. The modulation index of this antenna has been optimized to provide a quasi-uniform aperture field illumination [16]. Fig. 3(a) presents the radial evolution of the $\rho\rho$ component of the impedance tensor ($\phi = 0^o$) obtained with a constant periodicity and the optimized modulation index. In turn, Fig. 3(b) shows the efficiencies versus frequency. It can be

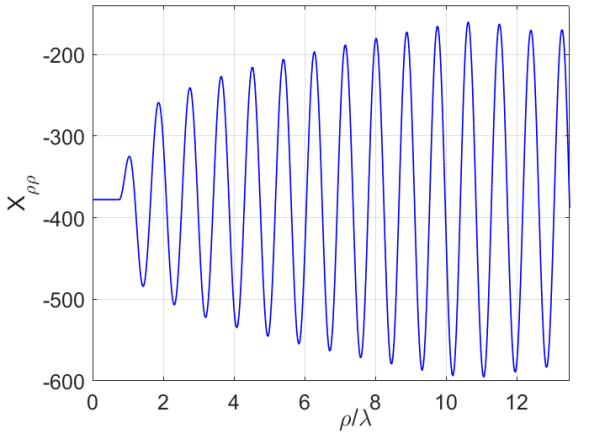

(a)

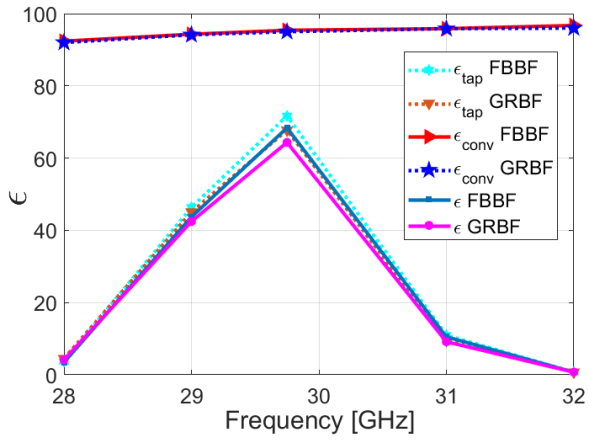

(b)

Fig. 3. Analysis of the efficiency for a uniform period MTS assuming that the frequency dispersion of the sheet is negligible. (a) cut of the impedance profile. (b) efficiency results. The global efficiency ϵ is the product between the aperture (tapering) efficiency ϵ_{tap} and the conversion efficiency ϵ_{conv}.

seen that the antenna bandwidth is not very large. Defining the bandwidth as the one corresponding to a drop of half of the maximum efficiency, the bandwidth of this antenna is about 6.5%. It is interesting to see that the global efficiency is mainly impacted by the aperture efficiency, the conversion efficiency being almost constant over a very large bandwidth.

As demonstrated in [9], the bandwidth can be improved by modulating the period of the reactance surface. Fig. 4(b) depicts the radial evolution of the $\rho\rho$ component of the impedance tensor ($\phi = 0^o$) for a modulated periodicity function. Fig. 4(b) shows the efficiency results of a broadside beam MTS designed to operate between 24 GHz and 30 GHz, i.e. 22% bandwidth. Differences between measurements and

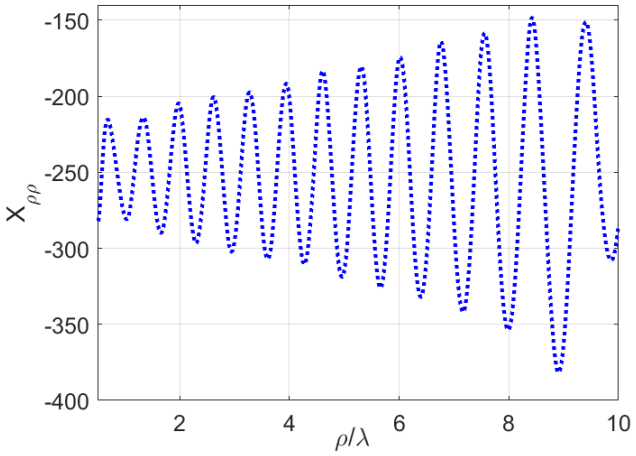

(a)

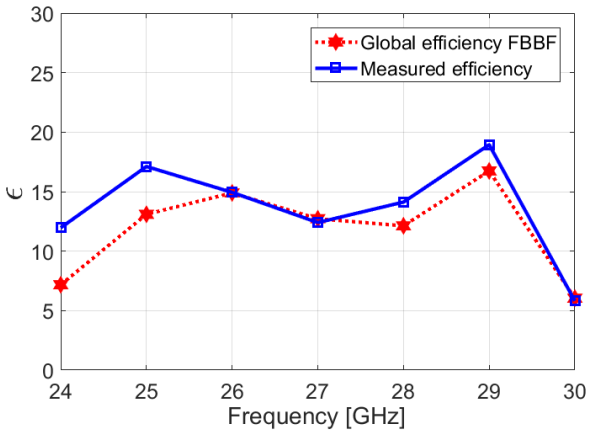

(b)

Fig. 4. Analysis of the efficiency for an active region MTS. (a) cut of the impedance profile. (b) efficiency results.

simulations can be attributed to the feeding modeling and the surface impedance implementation process with patches. In comparison with the uniform period MTS case, the global efficiency is lower due to the active region nature of the antenna. On average, the efficiency is 13% over a 22% bandwidth.

VI. Conclusion

We have presented two techniques for the analysis of the efficiency of MTS antennas. These two methods are based on completely different formalisms, but provide very similar

results and a very good agreement with commercial softwares and measured results. The impact on the efficiency when the bandwidth of the antenna is enlarged has been illustrated. It has been observed that the reduction of the global efficiency when one moves away from the center frequency is mainly due to the aperture efficiency, while the conversion efficiency has little impact. The algorithms presented in this paper can be used for the rapid and accurate optimization of the efficiency of MTS antennas designed with any synthesis technique, i.e the methods can handle arbitrarily modulated surface impedances. As such they provide to the antenna designer a reliable and efficient analysis tool.

ACKNOWLEDGMENT

This research has been partially funded by Région Wallonne through the LUMINET project under contract number 1810114.

REFERENCES

[1] O. Quevedo-Teruel et al. "Roadmap on metasurfaces," *J. Opt.*, vol. 21, no. 7, pp. 073002, July 2019.

[2] B. H. Fong, J. S. Colbrun, J. J. Ottusch, J. L. Visher and D. F. Sievenpiper "Scalar and tensor holographic artificial impedance surfaces," *IEEE Trans. Antennas Propag.*, vol. 58, no. 10, pp. 3212-3221, Oct. 2010.

[3] A. M. Patel, and A. Grbic, "Modeling and analysis of printed-circuit tensor impedance surfaces," *IEEE Trans. Antennas Propag.*, vol. 61, no. 1 pp. 211-220, Jan. 2013.

[4] G. Minatti, M. Faenzi, E. Martini, F. Caminita, P. De Vita, D. González-Ovejero, M. Sabbadini and S. Maci, "Modulated metasurface antennas for space: synthesis, analysis and realizations," *IEEE Trans. Antennas Propag.*, vol. 63, no. 4, pp. 1288-1300, April 2015.

[5] S. Pandi, C. A. Balanis, and C. R. Birtcher, "Design of scalar impedance holographic metasurfaces for antenna beam formation with desired polarization," *IEEE Trans. Antennas Propag.*, vol. 63, no. 7, pp. 3016-3024, Jul. 2015.

[6] G. Minatti, F. Caminita, E. Martini, M. Sabbadini and S. Maci, "Synthesis of modulated-metasurface antennas with amplitude, phase, and polarization control," *IEEE Trans. Antennas Propag.*, vol. 64, no. 9 pp. 3907-3919, Sep. 2016.

[7] M. Li, S. Xiao, and D. F. Sievenpiper, "Polarization-insensitive holographic surfaces with broadside radiation," *IEEE Trans. Antennas Propag.*, vol. 64, no. 12, pp. 5272-5280, Dec. 2016.

[8] M. Bodehou, C. Craeye, E. Martini, and I. Huynen, "A Quasi-direct method for the surface impedance design of modulated metasurface antennas," *IEEE Trans. Antennas Propag.*, vol. 67, no. 1, pp. 24-36, Jan. 2019.

[9] M. Faenzi, D. González-Ovejero, and S. Maci, "Wideband active region metasurface antennas," *IEEE Trans. Antennas Propag.*, vol. 68, no. 3, pp. 1261-1272, Sept. 2019.

[10] M. Bodehou, D. González-Ovejero, C. Craeye and I. Huynen, "Method of Moments simulation of modulated metasurface antennas with a set of orthogonal entire-domain basis functions," *IEEE Trans. Antennas Propag.*, vol. 67, no. 2, pp. 1119-1130, Feb. 2019.

[11] D. González-Ovejero and S. Maci, "Gaussian ring basis functions for the analysis of modulated metasurface antennas," *IEEE Trans. Antennas Propag.*, vol. 63, pp. 3982-3993, Sept. 2015.

[12] F. Verni, M. Righero and G. Vecchi, "On the use of entire-domain basis functions and fast factorizations for the design of modulated metasurface," *IEEE Trans. Antennas Propag.*, vol. 68, pp. 3824-3833, May 2020.

[13] M. Bodehou, et al, "Power balance and efficiency of metasurface antennas," *Sci. Rep.*, vol. 10, Oct 2020.

[14] M. Bodehou "Modulated metasurface antennas: analysis and direct numerical synthesis," *Ph.D thesis, UCLouvain*, March 2020.

[15] EM Software and Systems-S.A. (Pty) Ltd. (2014). FEKO: Field computations Involving Bodies of Arbitrary Shape, Stellenbosch, South Africa [Online]. Available: http://www.feko.info.

[16] M. Faenzi, et al, "Metasurface antennas: New models, applications and realizations," *Sci. Rep.*, vol. 9, pp. 1-14, July 2019.